DETECTION OF SKIN TUMORS ON CHICKEN CARCASSES USING HYPERSPECTRAL FLUORESCENCE IMAGING

I. Kim, M. S. Kim, Y. R. Chen, S. G. Kong

ABSTRACT. *This article presents a method for detecting skin tumors on chicken carcasses using hyperspectral fluorescence imaging data, which provide fluorescence information in both spectral and spatial dimensions. Since these two kinds of information are complementary to each other, it is necessary to exploit them in a synergistic manner. Chicken carcasses are examined first using spectral information, and the results are used to determine candidate regions for skin tumors. Next, a spatial classifier selects the real tumor spots from the candidate regions. It was shown that the method detected chicken carcasses with tumors, but failed to detect some tumors that were smaller than 3 mm in diameter. This study uncovered meaningful spectral bands for detecting tumors using hyperspectral imaging data. A detection system based on this method can improve the detection rate, and processing time can also be reduced, because the detection procedure is simplified by using a limited number of features, which reduces computational complexity. The resultant detection rate, false positive rate, and missing rate of the proposed method are 76%, 28%, and 24%, respectively*.

Keywords. *Classifier, Fluorescence imaging, Hyperspectral image, Skin tumor, Spectral and spatial information, Spectrum.*

The Food Safety and Inspection Service (FSIS) has a mandate to inspect each poultry carcass slaughtered and processed at poultry slaughter plants in the U.S. The USDA employs thousands of human inspectors to organoleptically inspect individual chicken carcasses on the processing lines. Each individual inspector typically examines 30 to 35 birds per minute (bpm) for shifts of up to 8 hours per day. Processing lines commonly run at 91 bpm, with some processing lines running at 140 bpm. A 91−bpm line presents every third bird to one inspector, thus requiring a total of three inspectors working in this manner to inspect all the birds. Inspectors working 8 hours per day in this noisy and highly humid environment have a tendency to develop repetitive motion injuries and fatigue problems (OSHA, 1999).

Thus, there is an urgent need to develop automated inspection systems that can operate on−line in real−time in the slaughter plant environment, at line speeds of at least 140 bpm. Researchers at the USDA Instrumentation and Sensing Laboratory (ISL) in Beltsville, Maryland, have been actively involved in developing on−line abnormality detection systems. Machine vision, multispectral imaging, and optical spectral systems for poultry inspection are among the approaches reported to differentiate wholesome from unwholesome chicken carcasses (Chen, 1993; Chen et al., 1998; Chao et al., 2002).

Hyperspectral imaging techniques have been utilized in many scientific disciplines, from microscopic studies to airborne remote−sensing applications (Martinsen et al., 1999; Shaw and Manolakis, 2002). A hyperspectral image is a three−dimensional (3−D) volume of data containing two−dimensional (2−D) spatial information measured at a sequence of individual wavelengths across a sufficiently broad spectral range. The resultant spectra can be used, in principle, to characterize and identify any given material. Recently, the ISL has developed a laboratory−based hyperspectral imaging system (Kim et al., 2001). It employs a pushbroom method in which a line of spatial information with a full spectral range per spatial pixel is captured sequentially along the other spatial dimension to construct a volume of hyperspectral imaging data.

A chicken skin tumor is a round, ulcerous lesion surrounded by a rim of thickened skin and dermis (Calnek et al., 1991). Tumors appear as small, scattered, localized shape deformations, with only slight discoloration. Conventional vision systems (i.e., reflectance) operating in the visible region are often too limited in sensitivity for adequate detection of skin tumors. Studies have shown that the presence of defects is more easily detected by using two or more spectral band images (Park et al., 1996; Wen and Tao, 1998). Detection of chicken skin tumors using multispectral reflectance imaging has also been reported by Chao et al. (2002), where each grid is classified based on statistical properties such as the coefficient of variation, skewness, and kurtosis of the surface reflectance in the grid.

Fluorescence is a phenomenon in which light absorption at a given wavelength by a fluorophore is followed by the emission of light at longer wavelengths. A number of

Article was submitted for review in December 2002; approved for publication by the Information & Electrical Technologies Division of ASAE in June 2004.

Company and product names are used for clarity and do not imply any endorsement by the USDA to the exclusion of other comparable products.

The authors are **Intaek Kim,** Professor, Department of Communication Engineering, Myongji University, Yongin, Kyonggido, South Korea; **Moon S. Kim,** Research Physicist, and **Yud−Ren Chen, ASAE Member Engineer,** Research Leader, USDA−ARS Instrumentation and Sensing Laboratory, Beltsville, Maryland; and **Seong G. Kong,** Associate Professor, Department of Electrical and Computer Engineering, University of Tennessee, Knoxville, Tennessee. **Corresponding author:** Yud−Ren Chen, USDA−ARS Instrumentation and Sensing Laboratory, Building 303 BARC−East, 10300 Baltimore Avenue, Beltsville, MD 20705−2350; phone: 301−504−8450; fax: 301−504−9466; e−mail: cheny@ba.ars.usda.gov.

compounds emit fluorescence in the visible region of the spectrum when excited with ultraviolet (UV) radiation (Chappelle et al., 1991). Fluorescence emission characteristics of food commodities can be changed by various factors. Exogenous contaminants, such as fecal contamination, as well as intrinsic changes in food products due to anomalies may lead to changes in the emission characteristics (Kim et al., 2001). However, the use of fluorescence measurements to date has not been fully explored for safety and quality inspection of chicken carcasses.

This article presents a novel method for detecting skin tumors on chicken carcasses. It utilizes both spectral and spatial information in hyperspectral fluorescence images. In order to increase the automated detection speed, a few simple features in both the spectral and spatial domains are selected for use as inputs for the decision−making procedure.

HYPERSPECTRAL IMAGING SYSTEM

The ISL hyperspectral imaging system used for the experiment is shown in figure 1. The key components of the system are a CCD camera, a spectrograph, a sample transport mechanism, and lighting sources. The CCD camera consists of a thermo−electrically cooled (three−stage Peltier device) electron multiplying charge−coupled device (EMCCD) with 288 (V) × 560 (H) pixels (Andor, Inc., South Windsor, Conn.). The spectrograph (ImSpector−V9, Spectral Imaging Ltd., Oulu, Finland) is based on prism−grating−prism (PGP) optics. Although the system is equipped with two independent illumination sources for reflectance and fluorescence imaging, only fluorescence hyperspectral images were used in this investigation. Two fluorescent lamp assemblies (model XX−15A, Spectronics Corp., Westbury, N.Y.) provide near−uniform UV−A (365 nm) excitation. Short−pass filters (UG1, Schott Glass Technologies, Duryea, Pa.) placed in front of the lamp housing prevent transmittance of radiation greater than approximately 400 nm, thus eliminating the potential detection of scattered excitation light as fluorescence.

For this investigation, 65 spectral−band images were used. Each image is a narrow band image whose center wavelength ranges from 425.4 to 710.7 nm at a uniform interval. Therefore, the center wavelength of the *k*th band image can be obtained from:

$$\lambda_k = 425.4 + (k - 1) \times (710.7 - 425.4) / 64 \text{ nm} \quad (1)$$

The spectral calibration was performed using spectral line lights (e.g., Hg and Ar). For a detailed description of the hyperspectral spectral imaging system and spectral calibration, see articles by Mehl et al. (2002) and Kim et al. (2001), respectively. A standard fluorescence target was measured prior to each experiment to ensure comparable fluorescence responses throughout this investigation. Line−by−line scans were achieved by moving the sample materials across the field of view via a precision positioning table.

HYPERSPECTRAL FLUORESCENCE IMAGES

Hyperspectral imaging yields a 3−D array or "cube" of data, stacking single−band images (each of size $M \times N$ pixels) along a spectral axis. Each data value represents the intensity of a pixel and can be denoted by $\mathbf{I}(u, v, \lambda)$, where $u = 1, 2, ..., M$, $v = 1, 2, ..., N$, and λ has a discrete value from λ_1 (425.4 nm) to λ_{65} (710.7 nm).

For a fixed λ_k, $\mathbf{I}(u, v, \lambda_k)$ represents the *k*th spectral band image, i.e., spatial information. If *u* and *v* are fixed, then $\mathbf{I}(u, v, \lambda)$ represents the spectrum at that pixel, i.e., spectral information. Images from two adjacent bands (λ_j and λ_{j+1}) are very similar because the spectral response of a pixel shows that there is rarely an abrupt change between two adjacent frequencies (wavelengths). On the other hand, images from distant bands can be much less similar and may have independent information. No single band image has sufficient information to describe the scene completely, which explains why hyperspectral images can be useful in the analysis of a scene.

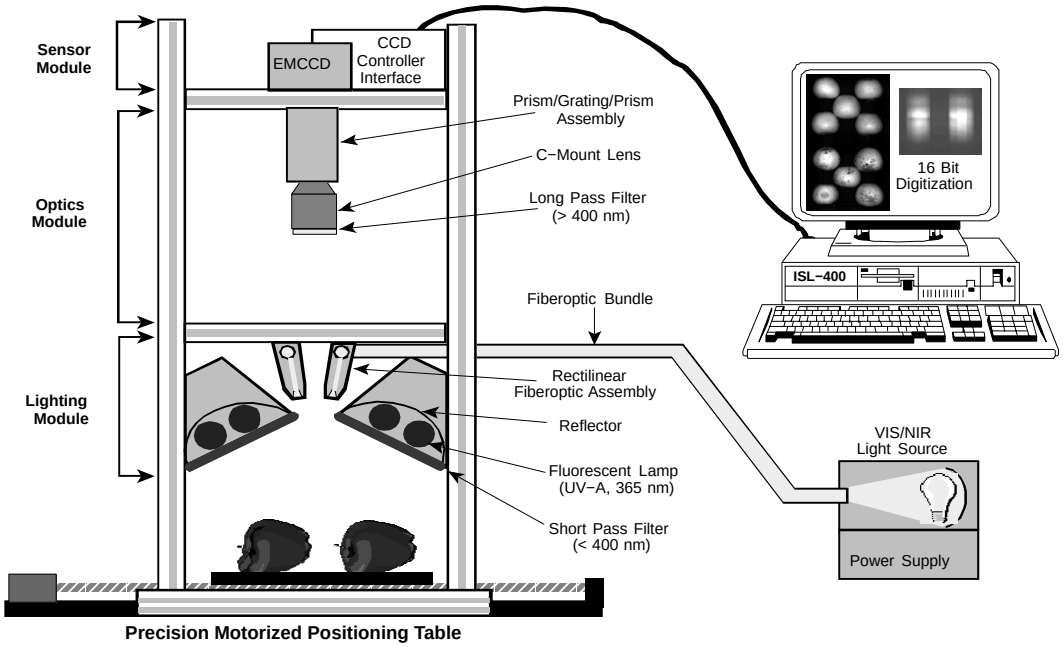

Figure 1. Schematic diagram of the ISL hyperspectral imaging system.

The 3−D array or "cube" of data, stacking single−band images along the spectral axis, is the output of the sensor (the hyperspectral imaging system). Features are measures used for the classification. In the more general case, n features (f_j,j = 1, 2, ..., n) are used, and they form the feature vector $\mathbf{f} = (f_1, f_2, ..., f_n)^T$, where T denotes transpose. There are many features in the hyperspectral image, and the dominant one is the intensity of a pixel from the various viewpoints. Feature selection is very important because a larger than necessary number of feature candidates exists in practice. In addition, some features are better than others in describing a certain object or phenomenon. Therefore, selecting optimal features is crucial for successful classification.

Most machine vision systems deal with a limited spectral range, but a single spectral band image may not contain adequate information for locating tumors. In comparison, hyperspectral imaging uniquely provides not only a range of spectral band images but also a spectrum for each pixel in an image. The spectral information at a pixel can work as a complement to the images. The proposed method in this article uses two kinds of classifiers, i.e., one spectral and one spatial, to take advantage of the complementary nature of these two different sources of information.

Preprocessing

The function of preprocessing is to obtain an ROI (region of interest) that contains only the chicken carcass image at each spectral band. In other words, the ROI excludes the background from the image. Removing the background can pose a problem in a single image due to difficulty in differentiating darker areas of chicken skin from the background. However, background removal becomes easy when several band images are available. Two steps are required. The first step is to obtain a threshold for each spectral image. The threshold is set at the intensity of the first minimal point (I_q) of the histogram from each image, assuming that the background is dark (a black, nonfluorescent background material was used in this study) and has a sizable area. The resultant binary image is given by equations $\mathbf{M}_q(u,v) = 1$ if $\mathbf{I}(u, v, \lambda_q) > I_q$ and $\mathbf{M}_q(u, v) = 0$ otherwise, where $\mathbf{M}_q(u, v)$ is the spatial image at λ_q. Then, applying a voting method to $\mathbf{M}_q$ using the following equations results in mask $\mathbf{M}(u,v)$:

$$\mathbf{M}(u,v) = 1 \text{ if } \sum_{q=1}^{Q} \mathbf{M}_q(u,v) > Q/2 \text{ for any } u \text{ and } v$$

$$\mathbf{M}(u,v) = 0 \text{ otherwise} \qquad (2)$$

where Q is the number of spectral bands. Now, new images, $\mathbf{I}_R(u, v, \lambda_j)$, which exclude the background are obtained by $\mathbf{I}_R(u, v, \lambda_j) = \mathbf{I}(u, v, \lambda_j) \times \mathbf{M}(u,v)$.

Spectral Classification

A classifier must be trained before it can perform classification. For training, selection of pixels from tumor areas and normal tissue areas was carefully carried out by visual inspection of hyperspectral and digital color images (ground truth) as displayed on a computer monitor.

Features were selected by evaluating spectral characteristics of the spectra shown in figure 4. By examining all the chicken spectra, with and without tumors, it was found that the most effective features that could differentiate tumor from normal skin are the intensity differences. For example, in figure 4, the intensity at band 20 can be a useful feature. The two classes, normal skin and tumor, have different intensity ranges, although some samples in each class overlap. Furthermore, based on wavelength−dependent fluorescence responses between the normal skins and tumors, a ratio of two bands can further amplify the differences between the two classes. Three distinctive (not optimal) features chosen based on the spectral responses were:

- f_1: maximum intensity (**I**) in bands [20, 25] (i.e., band 20 to band 25, inclusive) divided by 10,000.
- f_2: difference of intensities at band 10 and band 20 divided by 10,000.
- f_3: ratio of maximum **I** in bands [40, 45] to maximum **I** in bands [20, 25].

where the corresponding wavelength to band k can be calculated by equation 1. Each feature represents a value that can be dependent on the experimental condition. However, since the features have different values according to whether they belong to the normal skin class or tumor class, the values extracted from normal skin and tumor are clustered with different center points in the feature space, as shown in figure 5. Therefore, it can be concluded that the decision boundary of each feature is also dependent on the experimental condition and can be determined during the training phase and applied in the classification phase.

A fuzzy C−mean algorithm (Chi et al., 1996) is utilized to find the cluster centers and decision boundary. Using the training data, two clusters representing tumors and normal skins are constructed. The decision boundary is determined by a surface on which the membership grades for tumors (μ_{tumor}) and normal skins (μ_{normal}) are the same. The points on this surface are approximately equidistant from both cluster centers. The spectral classifier uses the decision boundary to classify a pixel into either the tumor or normal skin category.

Spatial Classification

The output of the spectral classifier is a spectral map ($\mathbf{I}_{sm}$) that shows the locations of potential tumors. A potential tumor is a region that consists of pixels identified as a tumor in spectral classification. The spectral classifier always yields more tumor spots (false positive) than actually exist because some normal areas are, spectrally, very similar to tumors. However, the opposite trend (false negative) in classification was not observed in this experiment. A spatial classifier that functions as a filter to pass tumors and block normal skins, based on the shape of potential tumors, can be used.

Shape has been the most dominant feature in conventional machine vision problems. The spectral classifier produces a spectral map ($\mathbf{I}_{sm}$) that shows the suspected area, and a spatial classifier pinpoints the tumors using the fact that most tumors have a round shape. It should be emphasized that the features are not obtained from any single image in the hyperspectral images, but from the spectral map, i.e., the result of the spectral classifier. The features extracted from the spectral map are area, major axis length, and minor axis length. These numbers are also found during the training phase.

Procedure Summary

Fusing spectral and spatial information leads to better accuracy because many single−method false positives can be rejected. In addition, the practical advantage of the fusion comes from the fact that it can simplify the procedures that are required in both spectral and spatial processing. Thus, fusion results in enhanced detection rate and reduced operation time as well.

The procedure for detecting tumors using both spectral and spatial information can be summarized as follows:

1. Read the captured images and construct hyperspectral images $\mathbf{I}(u, v, \lambda)$.
2. Remove background. Set $\mathbf{M}(u, v) = 1$ for the region of interest and $\mathbf{M}(u, v) = 0$ for the background.
3. Use spectrum $\mathbf{I}(u, v, \lambda)$ as an input to a spectral classifier. The decision rule of the classifier is explained in the spectral classification. The output, called a spectral map ($\mathbf{I}_{sm}$), is the resultant image of the classifier. Each pixel satisfies the criteria of the spectral classifier.
4. Use the spectral map ($\mathbf{I}_{sm}$) as an input to a spatial classifier that is detailed in the spatial classification. The criteria of the classifier are structural properties such as size, filling ratio, and ratio of major to minor axes.
5. The output of the spatial classifier shows the locations of tumors detected.

Testing the Methodology

Samples

A total of 13 chicken carcasses with skin tumors were collected from a poultry processing plant (Allen Family Foods, Inc., Cordova, Md.) in March and May 2002. The conditions of the chicken carcasses were identified by the FSIS veterinarian at the plant. Tumors on the birds included early and advanced tumor stages, ranging from very small (less than 3 mm in diameter) to large (more than 10 mm in diameter) in size. Samples were put in plastic bags to minimize dehydration and then placed in a cooler with ice. The carcasses were transported to ISL within two hours, and imaging measurements were conducted on the same day. Individual tumor spots on the samples were marked with labels, and digital color images of whole birds were acquired.

Results

Twelve of 65 spectral band images of the same carcass, each image 400 × 460 pixels in size, are shown in figure 2. Unlike the usual gray−level image from a typical CCD camera, the intensity level at each pixel reflects the fluorescence characteristics at a specific wavelength. The background is removed in this stage of preprocessing. A typical mask **M** for the ROI, obtained as described in the preprocessing section, is shown in figure 3.

A total of 113 pixels (65 normal skin and 48 tumor) from 13 chicken carcasses were chosen for training. The spectra are shown in figure 4. The feature vector has three components (f_1, f_2, and f_3). Then, f_1 = maximum intensity in bands [20, 25] / 10,000, f_2 = slope in bands [10, 20] / 10,000, and f_3 = maximum intensity in bands [40, 45] / maximum intensity in bands [20, 25]. The relationship between feature f_1 and feature f_3 is shown in figure 5. Two clusters can be seen fairly well separated but lacking perfect separation. To classify every pixel in the ROI, each pixel goes through the spectral classifier that is based on a fuzzy C−mean algorithm (Chi et al., 1996). The algorithm results in the center of each cluster in 3−D feature space at the coordinates (0.59, 0.44, 0.80) and (0.89, 0.19, 0.33) for normal skin and tumor, respectively. The decision rules are as follows:

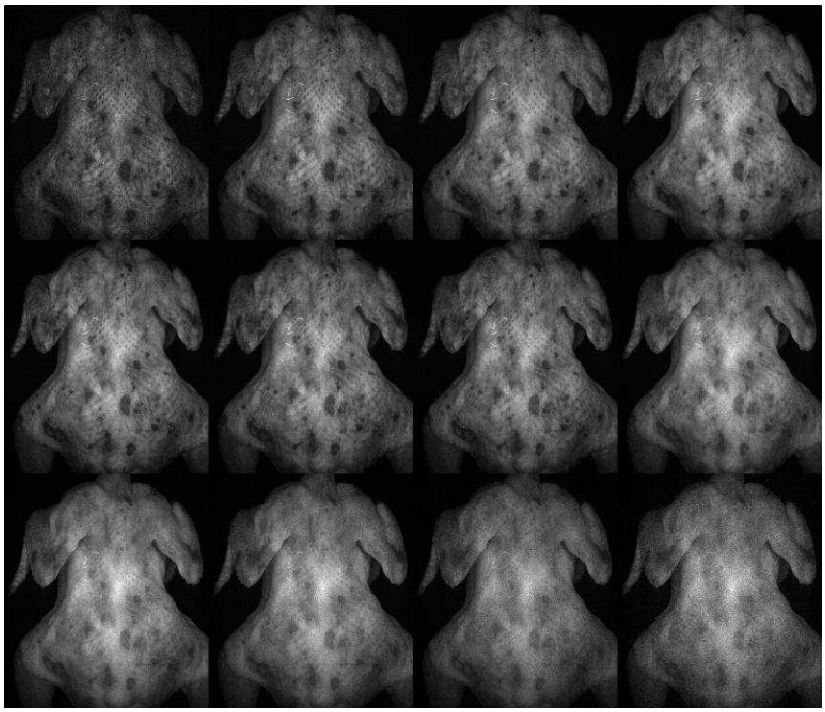

Figure 2. Hyperspectral fluorescence images with various λ_k values (k = 5, 10, 15, ..., 60) from left to right, top to bottom, where $\lambda_{5n} = 420.9 + 5n \times 4.46$ (nm).

Figure 3. Mask showing the region of interest.

If $f_1 \in$ tumor, $f_2 \in$ tumor, and $f_3 \in$ tumor,
then the pixel is a tumor.

Otherwise, the pixel is normal. (3)

where $f \in$ tumor indicates that the fuzzy membership grade of f being tumor is greater than that of normal.

For validation, a total of 110 pixels were selected and the decision rules were applied. This yielded:

P(tumor|normal) = 6/70
P(normal|normal) = 64/70
P(normal|tumor) = 2/40
P(tumor|tumor) = 38/40

where

P(tumor|normal) is the conditional probability of tumor given normal skin, i.e., the probability of declaring tumor given that tumor is not present, a false positive,

P(normal|normal) is the probability of declaring normal skin given that tumor is not present,

P(normal|tumor) is the probability of declaring normal skin at an actual tumor spot, and

P(tumor|tumor) is the probability of declaring tumor given that tumor is present.

These conditional probabilities indicate that there is no perfect decision boundary satisfying even the training set. Therefore, it is no surprise that misclassification can frequently happen when test data are applied to the spectral classifier. The spectral map ($\mathbf{I}_{sm}$), shown in figure 6, is both the output of the spectral classifier and the input of the spatial classifier. One reason for misclassification is that the selected spectral features are incomplete to describe all pixels. It was observed in this experiment that some normal skins have spectral characteristics similar to those of tumors, to a certain degree. Thus, some normal skins may be spectrally misclassified. Additional information is needed to further classify tumors correctively.

Many spots falsely identified as tumors can be filtered out by using spatial/structural information. In this experiment, two features were examined: the ratio of major axis to minor axis (R) and the number of pixels in tumor area (A). During the training phase, tumors were found to satisfy both conditions: $R < 2$, and $90 < A < 900$. Employing this rule using the spatial classifier, the resultant output is shown in figure 7.

Detection results are summarized in table 1. Images 1 through 6 and image 10 have one carcass in each image,

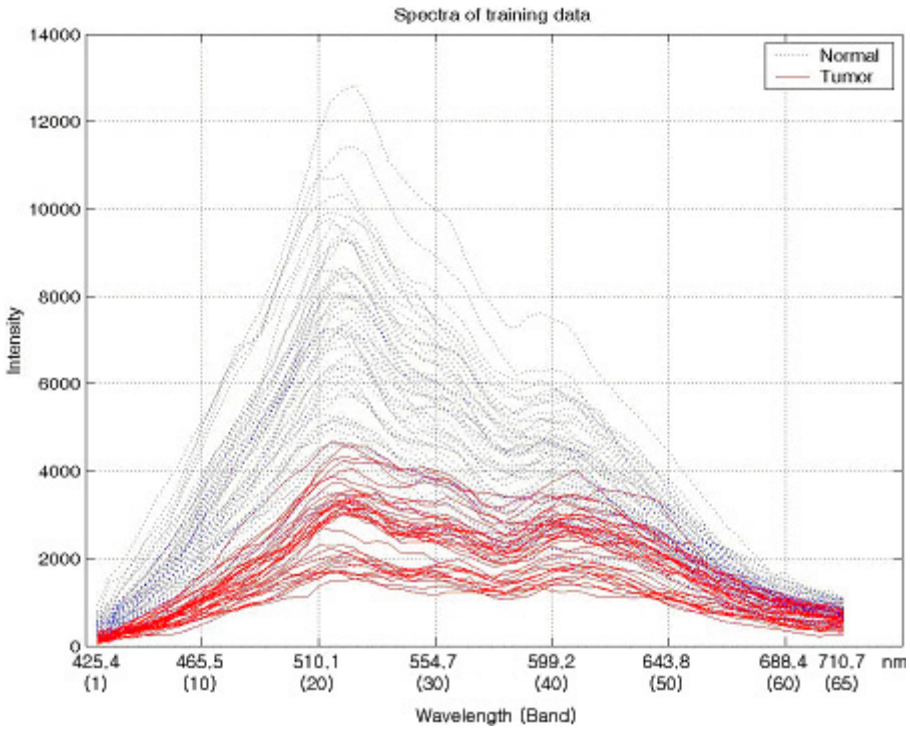

Figure 4. Spectra of training data.

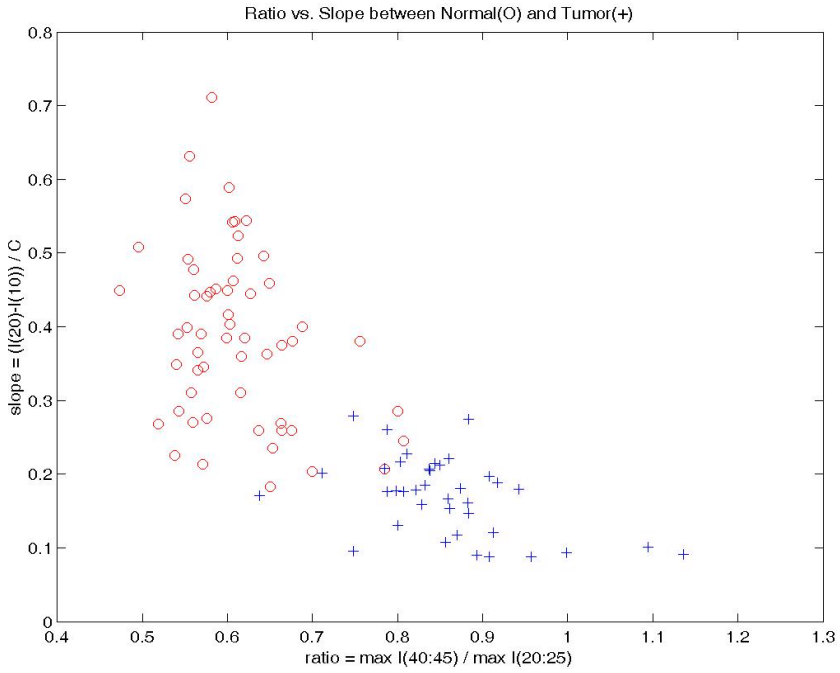

Figure 5. Ratio of maximum intensity vs. slope between normal and tumor in training data.

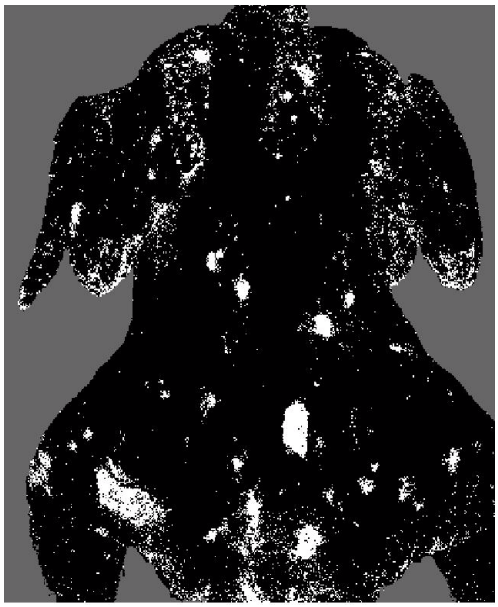

Figure 6. Spectral map I_{sm}.

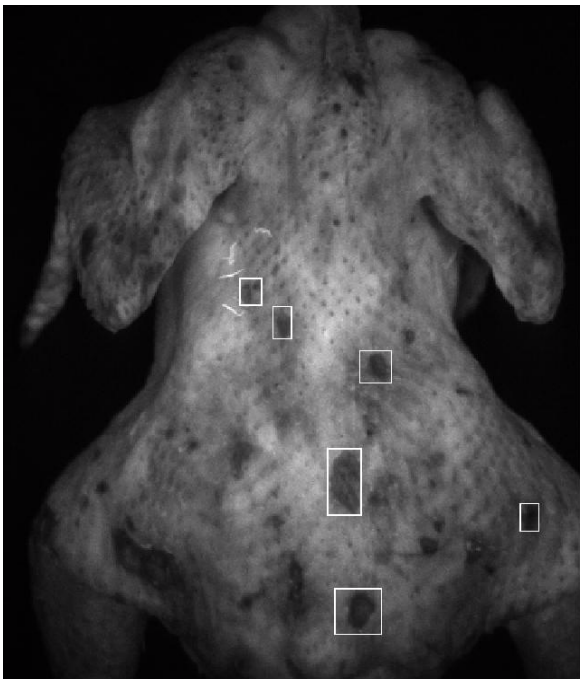

Figure 7. Detection result (regions marked by rectangles are classified as tumors).

whereas images 7, 8, and 9 contain two carcasses each. The rate for detecting actual tumors is 76%, for false positives is 28%, and for actual tumors missed is 24%. However, all 13 chicken carcasses with tumors are identified as having tumor spots. Observation has shown that isolated tumors are easily detected as long as they are larger than 3 mm in diameter, but detection failure is likely to occur when tumors are close together. A relatively high rate of missed tumors is also attributed to one chicken sample (image 10) with multiple early−stage tumor spots smaller than 3 mm in diameter.

DISCUSSION

In this study, tumors were detected using both spectral and spatial information in hyperspectral fluorescence images. Using different types of information or sensors is a well−known methodology called sensor fusion that pursues extracting the greatest amount of information possible in the sensed environment (Waltz and Llinas, 1990; Kim, 1992). The advantages of sensor fusion come from using the different sensors or information synergistically, and typically include reduced processing time and improved decision accuracy. The spectral classifier or the spatial classifier alone cannot detect tumors because, individually, the spectral information and the spatial information are each incomplete in describing tumors. But using both pieces of information, the

Table 1. Detection results.

Image	No. of Real Tumors	No. of Detections	No. of False Positives	No. of Missing
1	3	3	1	0
2	3	3	0	0
3	1	1	1	0
4	3	2	1	1
5	4	4	1	0
6	2	1	1	1
7 (2)[a]	3	3	1	0
8 (2)	7	5	3	2
9 (2)	3	3	3	0
10	12	6	0	6
Total	41	31 (76%)	12 (28%)	10 (24%)

[a] Number of chicken carcasses contained in the image.

classification rule for detecting tumors can be loosely defined in terms of both the spectral and spatial domains. Consequently, processing time can be reduced due to the less complex classification rules, and detection accuracy can be improved owing to the complementary natures of spectral and spatial searches.

Optimal features can be defined as those that maximize the distance measure between different classes. However, in reality, "good features" that yield an acceptable classification rate for the validation data set are sought instead of optimal features. This is because analytically countless searches (iterative) are needed before the optimal features are obtained. For example, from among 65 bands (wavelengths), any numerical combination of band intensities can represent a feature. Therefore, finding optimal features, a popular topic covered in the pattern recognition area, requires more rigorous effort and is not elaborated upon in this article. However, spectral−based assessment provides a means to determine several features. In addition, considering the results achieved from applying the selected features to the validation data set, the features based on differences in fluorescence response between normal skins and tumors were adequate to avoid the time−consuming (iterative) process of finding optimal features.

The number of chickens used in this study may raise a concern in terms of the sample size, in that a total of 13 chickens may seem too small to generalize the proposed method. However, the algorithm is not applied to whole chickens but to individual pixels. Considering that each image is 400 × 460 pixels, classifications are performed at least 184,000 times for each image. The training samples (113 pixels) were selected from about 1,840,000 pixels (10 images), and 110 pixels were used for the validation data set. There was no overlap between the training and validation data sets. This is one of the advantages of using imaging techniques, in that large numbers of sample pixels are available to evaluate the method.

Conclusions

This article presents a novel method for detecting skin tumors on chicken carcasses. It uses both the spectral and spatial information in hyperspectral fluorescence images in a synergistic manner. The method first finds a mask that contains only the region of interest (e.g., chicken carcasses). A voting method is utilized to determine if a pixel is a member of either the background or the ROI from each binary band image. A spectral classifier produces a spectral map that locates the potential tumorous regions based on the selected features. Examining the spectral map with criteria for spatial characteristics of tumors yields final results that show the location of tumors. The detection rate, false positive rate, and missing rate were 76%, 28%, and 24%, respectively. It was found that the detection rate is more sensitive to the decision rules of the spatial classifier than to those of the spectral classifier.

There are some issues that need to be considered for future work to produce better results. The most important issue is to devise a method of optimal feature selection. The optimal set of features will find a better decision boundary that can minimize erroneous classification. Another possibility for improving the detection rate can be found via the enhancement of spectral map $\mathbf{I}_{sm}$. Compared with chicken carcasses, the map shows some spots that are irrelevant to tumors, and some of them are not filtered out in the spatial classifier, causing a high false positive rate.

Acknowledgements

The authors would like to thank Dr. Sukwon Kang of ISL for his comments in experiment and data analysis, Mr. Frank Gwozdz of ISL for his assistance in sample collection, and Ms. Diane Chan of ISL for her technical assistance and proofreading of the manuscript.

References

Calnek, B. W., H. John Barnes, C. W. Beard, W. M. Reid, and H. W. Yoder. 1991. *Diseases of Poultry.* Chapter 16, 386−484. Ames, Iowa: Iowa State University Press.

Chao, K., Y. R. Chen, W. R. Hruschka, and F. B. Gwozdz. 2002. On−line inspection of poultry carcasses by a dual−camera system. *J. Food. Eng.* 51(3): 185−192.

Chappelle, E. W., J. E. McMurtrey, and M. S. Kim. 1991. Identification of the pigment responsible for the blue fluorescence band in laser−induced fluorescence spectra of green plants, and potential use of this band in remotely estimating rates of photosynthesis. *Remote Sens. Environ.* 36(3): 213−218.

Chen, Y. R. 1993. Classifying diseased poultry carcasses by visible and near−IR reflectance spectroscopy. *Optics in Agriculture and Forestry,* SPIE 1836: 46−55.

Chen, Y. R., B. Park, R. W. Huffman, and M. Nguyen. 1998. Classification of on−line poultry carcasses with backpropagation neural networks. *J. Food. Proc. Eng.* 21(1): 33−48.

Chi, Z, H. Yan, and T. Pham. 1996. *Fuzzy Algorithms: With Applications to Image Processing and Pattern Recognition*. River Edge, N.J.: World Scientific.

Kim, I. 1992. A hybrid analytical/intelligent methodology for sensor fusion. PhD diss. Atlanta, Ga.: Georgia Institute of Technology.

Kim, M. S., Y. R. Chen, and P. M. Mehl. 2001. Hyperspectral reflectance and fluorescence imaging system for food quality and safety. *Trans. ASAE* 44(3): 721−729.

Martinsen, P., P. Schaare, and M. Andrews. 1999. A versatile near−infrared imaging spectrometer. *J. Near−Infrared Spectrosc.* 7(1): 17−25.

Mehl, P. M., K. Chao, M. S. Kim, and Y. R. Chen. 2002. Detection of contamination on selected apple cultivars using hyperspectral and multispectral image analysis. *Applied Eng. in Agric.* 18(2): 219−226.

OSHA. 1999. Chicken disassembly − Ergonomic considerations. Washington, D.C.: U.S. Department of Labor. Available at: www.osha.gov/SLTC/poultryprocessing.

Park, B., Y. R. Chen, M. Nguyen, and H. Hwang. 1996. Characterizing multispectral images of tumorous, bruised, skin−torn, and wholesome poultry carcasses. *Trans. ASAE* 39(5): 1933−1941.

Shaw, G., and D. Manolakis. 2002. Signal processing for hyperspectral image exploitation. *IEEE Signal Processing Magazine* (Jan.): 12−16.

Waltz, E., and J. Llinas. 1990. *Multisensor Data Fusion*. Norwood, Mass.: Artech House.

Wen, Z., and Y. Tao. 1998. Fuzzy−based determination of model and parameters of dual−wavelength vision system for on−line apple sorting. *Optical Eng.* 37(1): 293−299.